Optical properties of a nanomatch-like plasmonic structure

Xudong Cui,[1,2,*] Weihua Zhang,[3] Daniel Erni,[2] and Lixin Dong[4]

[1]*Department of Material Science and Technology, Research Center of Laser Fusion, China Academy of Engineering Physics, Sichuan 621900, China*
[2]*General and Theoretical Electrical Engineering (ATE), Faculty of Engineering, University of Duisburg-Essen, and CeNIDE–Center for Nanointegration Duisburg-Essen, D-47048 Duisburg, Germany*
[3]*Nanophotonics and Metrology Laboratory, EPFL, Lausanne CH-1015, Switzerland*
[4]*NanoRobotic Systems Laboratory, Michigan State University, East Lansing, Michigan 48824, USA*
[*]*Corresponding author: xudong.cui@uni-due.de*

Received March 19, 2010; revised June 8, 2010; accepted June 11, 2010;
posted June 14, 2010 (Doc. ID 125698); published July 9, 2010

The optical properties of a match-like plasmonic nanostructure are numerically investigated using full-wave finite-difference time-domain analysis in conjunction with dispersive material models. This work is mainly motivated by the developed technique enabling reproducible fabrication of nanomatch structures as well as the growing applications that utilize the localized field enhancement in plasmonic nanostructures. Our research revealed that due to the pronounced field enhancement and larger resonance tunabilities, some nanomatch topologies show potentials for various applications in the field of, e.g., sensing as well as a novel scheme for highly reproducible tips in scanning near field optical microscopy, among others. Despite the additional degrees of freedom that are offered by the composite nature of the proposed nanomatch topology, the paper also reflects on a fundamental complication intrinsic to the material interfaces especially in the nanoscale: stoichiometric mixing. We conclude that the specificity in material modeling will become a significant issue in future research on functionalized composite nanostructures.

OCIS codes: 230.0230, 240.6680, 250.5403.

1. INTRODUCTION

Metallic nanoparticles exhibiting characteristic optical properties caused by the excitation of localized surface plasmon resonances [1–4] are widely used, e.g., in biosensing [2], drug delivery [3], and biomedical imaging [4]. With the rapid development of nanofabrication processing [5–8], as well as the progress in corresponding characterization and measurement technologies, not only simple nanoparticles such as, e.g., spherical particles, but also hybrid nanostructures such as, e.g., nanoshells (nanorices) [9], nanocups [10], semi-shells [11], and nanocrescents [12] can be synthesized by physical and chemical methods. Their optical properties are intensively exploited, displaying promising features such as, e.g., large tuning ranges for surface plasmon resonances reaching from the near infrared to ultraviolet wavelengths, high sensitivities against various properties of the surrounding media, and large local field enhancements [8–12]. Some of these novel properties are arising from the reduced symmetry of their geometries, and therefore motivated increasing research efforts in developing new yet complicated structures like multiblock nanostructures [13] and multisegment nanowires [7,14,15]. These metal-semiconductor heterostructures exhibited exceptional optical properties compared to other shaped nanoparticles in terms of controllability of surface plasmon resonances, multiplex sensing, and unidirectional surface plasmon-polariton propagation.

In this paper, we investigate the optical properties of a new plasmonic structure—the nanomatch—a quasi-one-dimensional metallo-dielectric nanostructure using numerical simulations based on the finite-difference time-domain (FDTD) method [16]. The focuses are on the optical properties of the nanomatch structures as functions of the length l of the matchstick, the shape of the match end (i.e., cut depth h), the polarization, as well as the corresponding material properties. Our investigations suggest that due to its pronounced field enhancement, large resonance tunabilities, as well as its mature fabrication techniques for reproducibility, the nanomatch structure is well suited for potential applications in biomolecule detection, with sensing, and as a tip for scanning near field microscopy or tip-enhanced Raman spectroscopy (TERS) [17]. Additionally, the nanomatch structure reported here results in a distinct nanoscale metal-semiconductor contact that may become well suited in the context of future ultra-dense chip-interconnects [5].

2. NANOMATCH STRUCTURE

Figure 1 shows the transmission electron microscopy (TEM) image of a fabricated nanomatch structure that has been fabricated using nanorobotic spot welding developed by one of the authors [8]. One end of the match is made of a hemispherical-like metallic structure, whereas the matchstick consists of a straight rod made of either dielectric or metal that is attached at the flattened part of the nanoscopic hemisphere. Owing to the advanced fabrication technology other shapes such as conical rods are also possible. By altering the fabrication procedures, one

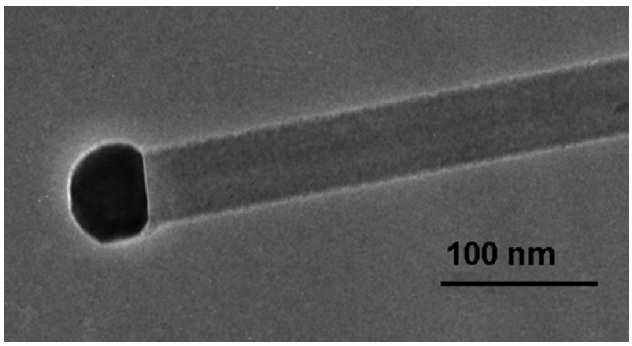

Fig. 1. TEM image of the fabricated nanomatch structure. The dark part corresponds to the metallic end of the match that is spliced to the matchstick made of dielectric material. The diameter of match end is about 60 nm with a cut depth of $h=10$ nm; the diameter of the matchstick is about 46 nm.

can replace the dielectric part with a metal to set up a metallic heterostructure that is useful for, e.g., contacting electrodes in nanocircuits [5]. In this work, we will numerically investigate the optical properties of the nanomatch structure, where the material of the matchstick is either silica or gold, and the match end is assumed to be gold throughout all the analysis. Noble metals like gold are widely used at optical frequencies due to both the small losses and the fact that gold is chemically inert under ambient conditions.

3. SIMULATION PRELIMINARIES

Our numerical analysis is carried out using the three-dimensional FDTD-based full-wave simulation code [16]. The nanomatch structure consists of a nanowire joint to a truncated metallic nanosphere entailing a small curvature; and the overall nanostructure is embedded in air. It is challenging to simulate such particularly shaped structures at optical frequencies just with conventional FDTD methods due to discretization effects in the underlying orthogonal and staggered grids, which commensurate with the Cartesian coordinate system [18]. Therefore, additional modifications such as improved conformal algorithms using structured meshes [19] are needed in order to improve the numerical accuracy when dealing with curved structures, and in particular with curved interfaces between different materials. In computer simulation technology (CST), a perfect boundary approximation is used to increase the resolution of curved meshes [16]. In addition to the meshing schemes, modeling dispersive materials with curved surfaces still remains to be challenging due to both the complexity in algorithms and the introduction of potential numerical instability in the FDTD computation. A simple solution to the aforementioned instability problem is to use the so-called "effective permittivities" [20] that provide a volumetric treatment of curved boundaries in the Cartesian discretization scheme. To conduct reliable simulations, we used experimental frequency-dependent data for the corresponding metals. The measured data are fitted to a Drude model, where it is easily adaptable to the convolution integral algorithms in FDTD. The measured complex dielectric permittivities for gold [21] and the corresponding fitted models are shown in Fig. 2. Note the differences between

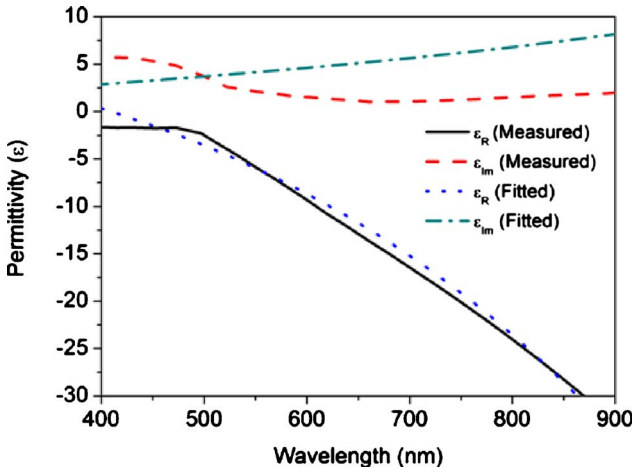

Fig. 2. (Color online) Spectral response of the permittivity of gold used in our calculations showing both the measured data and the fitted model data for comparison.

these two data sets: smaller deviations exist for the real parts of these two models within the wavelength of interest, while the imaginary parts show larger differences when the wavelengths are close to the resonance of bulk gold material. Since the imaginary part always indicates the presence of losses in the material, the derived field in the structure is underestimated for wavelengths larger than 500 nm and is otherwise overestimated below wavelengths of 500 nm when using the fitted material model (Fig. 2). We have compared the two data sets (measured and fitting models) in a frequency domain calculation for a 20 nm gold sphere [1] and found that the resulting resonances are separated by 2 nm and the electric field enhancements are differing by 11% in amplitude. Therefore, finding better-adapted fitting models that are even transferable into time-domain representations still remains a challenging task. However, the built-in functions in CST do not support the flexibility of using different fitting models to the measured data, which should be kept in mind when comparing the results with the ones stemming from different codes. In the presented work, namely, throughout all the corresponding simulations, we will refer our material models for gold to the fitted data as displayed in Fig. 2.

The overall simulation domain is truncated and surrounded with perfectly matched layers (PMLs) yielding separation distances of 200 nm between all such boundaries and the nanomatch structure. We use four-layer convolution perfectly matched layers (CPMLs) with reflection coefficients below 0.0001 in order to minimize undesired spurious reflections in the calculations. The new CPML formulation in CST [16] also provides a material-independent absorbing boundary condition, namely, if electric, magnetic, and conducting material properties are considered to improve the absorption efficiencies. Besides the boundary conditions, mesh generation is an important issue when using CST. The mesh is linearly graded with a 10:1 ultimate ratio; i.e., if the grid cells in the immediate vicinity of the nanomatch have typical sizes of around $\sim$0.1 nm on each side, the cells on the outer boundary of the simulation volume will have dimensions on the order of $\sim$1 nm. Mesh cells as small as 0.1 nm are used in our

simulations. Evidently, this will lead to a large number of grid cells. To reduce the memory requirements and computation time, symmetry planes are introduced either as an electric wall (i.e., a perfect electric conducting plane) or as a magnetic wall (i.e., perfect magnetic conducting plane). The simulations are run on an Intel quad core processor (3 GHz) with 32 Gbytes random access memory, with typical runtimes on the order of several tens of hours.

As can be observed in Fig. 1 the displayed end of the nanomatch has a reduced symmetry compared to the spherical particle; hence its optical properties might become polarization dependent. In the present work, we consider two polarization directions with respect to the axis of the nanomatch (i.e., the y direction, which also defines the corresponding orientation of the non-spherical match end) for the plane wave excitation incident along the x direction having, thus, either an E_y or E_z polarization, while for the structures with a fully developed matchstick only E_y polarization is used. A typical end region of the nanomatch, i.e., the non-spherical match end, is shown in Fig. 3 together with an equally sized sphere for comparison reasons. The radius R is set to 10 nm throughout the simulations and the cut depth h is varied and can be precisely controlled during the fabrication. The proper radius of the matchstick is therefore a function of h and is governed by the simple geometrical relation

$$r = \sqrt{R^2 - (R-h)^2} = \sqrt{2Rh - h^2}. \quad (1)$$

In the following section, the optical properties of the nanomatch structures are investigated as functions of the cut depth h, the length of the matchstick l, the shape of the matchstick, as well as the material properties of the matchstick where the thickness of the latter is based on the structural relations provided in Eq. (1).

4. RESULTS AND DISCUSSION

A. Optical Properties of the Metallic Match End

The spectral responses of the scattering cross section (SCS) of the match end are shown in Fig. 4. The resonance of a single sphere (i.e., a match end with a cut depth of $h=0$ nm) was found at a wavelength of 525 nm in the visible spectrum where the underlying material properties correspond to the fitted model (cf. Fig. 2) as implemented in CST. Note that the resonance of a single spherical nanoparticle can be analytically predicted in the framework of Mie theory [1]. For instance, the resonance

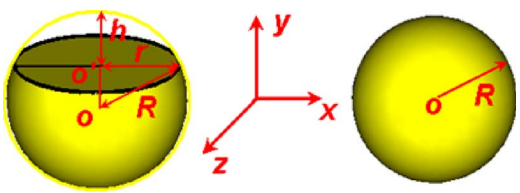

Fig. 3. (Color online) Schematic drawing of the nanomatch end. The non-spherical match end is displayed on the left where the cut part is later joined to the matchstick. The right picture shows a metallic sphere for comparison. The radius of the metallic sphere is $R=10$ nm, whereas the cut depth is termed h as indicated in the figure.

wavelength of a gold sphere with a diameter of 20 nm amounts to 523 nm where the optical properties of gold are given by the well-known reference data from Johnson and Christy [21]. The resulting 2 nm discrepancy between the two resonance wavelengths is due to a minor mismatch of the fitted permittivity model with respect to the reference data as shown in Fig. 2. Nevertheless, this will have no significant impact on our further analysis of the different nanomatch configurations as long as we stick to the same material model. From Fig. 5(a) we observed that for a y-polarized plane wave excitation (E_y), the electric field strength at the match end's bulge obeys an overall decreasing tendency with respect to the increasing cut depth h. This can be attributed to a redistribution of charge toward the cut edge at the expense of the charge density at the proper bulge.

It is worth noting that in some codes such as, e.g., the boundary element methods, the cut edges are necessarily rounded to avoid numerical instabilities due to emerging field singularities at the proper edges [22]. Standard implementations of FDTD are hardly affected by those sharp edges due to the inherent lack of resolution in the underlying domain discretization schemes (i.e., the staggered meshes in the Cartesian coordinate systems) [18]. However, if unstructured meshes based on, e.g., hexahedral or tetrahedral meshes were used in the FDTD scheme, one has inevitably to rely on linear approximations for the object shapes in these regions in order to avoid inverted elements, where the latter seem likely to provide extremely dense meshes and, hence, an intractably large number of degrees of freedom. In order to foster stability in the subsequent simulations all emergent edges within the nanomatch configurations are rounded according to a 1 nm radius.

In this study the resonances of the match end are of particular interest. Typically, the partial removal of metal results in a slightly redshifted resonance compared to the spherical particle for cut depths h approaching 10 nm. This is evident from Fig. 4(a) for E_y polarization where the resonance wavelengths amount to 526, 527, 528, and 530 nm for the corresponding cut depths of 2, 4, 6, and 10 nm, respectively. An exception to the displayed behavior is provided at a cut depth of 8 nm, where the resonance wavelength bounces with 522 nm even below the resonance of the spherical particle. When the cut depth h reaches 16 nm, the significant resonance continues to redshift again while a smaller resonance peak has emerged on the high-energy side.

For E_z polarization, the electric field strengths at the match end's bulge are lowered due to the change in polarization directions, and for increasing cut depths below 7 nm the resonance wavelengths become decreasingly blueshifted compared to the resonance of the spherical particle [cf. Fig. 4(b)]. Interestingly, at $h=7$ nm the resonance wavelength approaches the value for the spherical particle, whereas for larger cut depths the redshift continues. The anomaly that occurs here at around $h=8$ nm behaves contrary to the case of y-polarization, showing a swing toward 542 nm, which lies significantly above the resonance wavelength of the spherical particle. For deeper cuts, i.e., $h>10$ nm, only a barely visible indication for additional resonances is found in the spectrum. These behaviors are

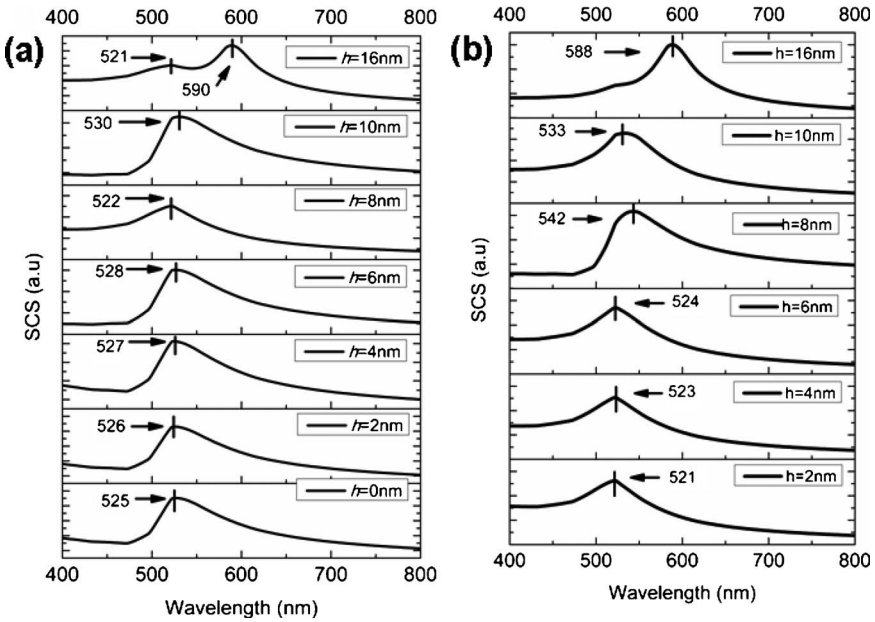

Fig. 4. The spectral response of the SCS for different match ends as a function of cut depth h. The resonances are identified by bold dashes and accordingly labeled with the corresponding wavelengths. The SCSs are displayed (a) for a y-polarized plane wave excitation and (b) for a z-polarized plane wave excitation (cf. Fig. 3).

different compared to semi-shell structures with comparable diameters as reported in [11], where additional resonances will evolve at some wavelengths depending on the removal of the conducting material. A straightforward interpretation of the reported spectral behavior becomes very challenging since mode hybridization concept [23] is not applicable here for such nanomatch structures. One of the main reasons is that because the mode hybridization concept implies electromagnetic interaction between the modes of two (or more) different objects (such as a nanosphere and a nanocavity as observed in the case of plasmonic nanoshells or two closely located nanoparticles or optical microcavities), which results in the mode splitting into symmetric or "bonding" modes and antisymmetric or "antibonding" modes, while the symmetry-breaking deformation of the spherical particle shape considered here simply results in lifting the degeneracy of the dipole mode and thus in the appearance of additional peaks in the particle spectrum. The reported anomalous wavelength shifts are thus believed to originate from such a symmetry-breaking of spherical shapes, which then finally tends to evolve into the resonance splitting for large cut depths.

However, the mode coupling is not so strong due to the small particle size compared to the operating wavelengths. Note that the apparent polarization sensitivity is mainly supported by structures with a reduced symmetry [11] as displayed in Fig. 5, where the electric field patterns at resonance are shown for the nanomatch end according to the various cut depths h. From the field patterns, one can observe that a dipolar behavior is generally present at resonance where higher order modes start to emerge for cut depths $h > 14$ nm.

B. Nanomatch with a Cylindrical Dielectric Matchstick

As shown in Fig. 1 the overall nanomatch structure comprises the previously discussed match end together with a cylindrical dielectric rod of circular cross section as illus-

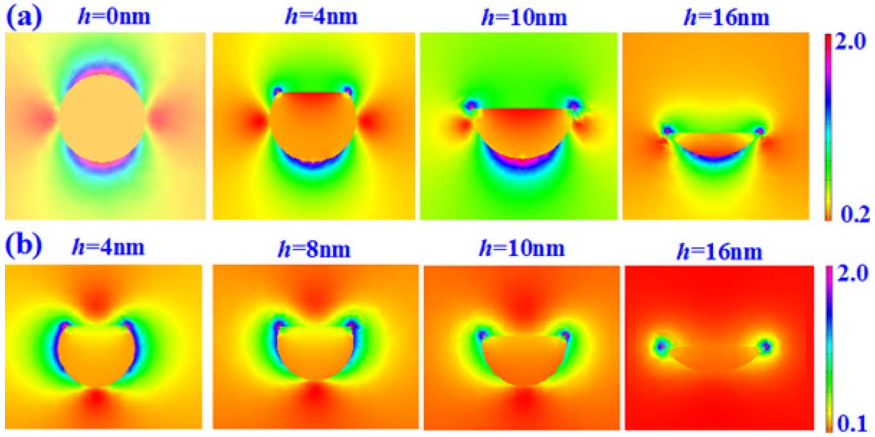

Fig. 5. (Color online) Electric field strength at the resonances corresponding to the indicated cut depth h of the match end for (a) y-polarization and (b) z-polarization.

trated in the inset of Fig. 6. The dielectric rod (i.e., the matchstick) is made up of silica with $\varepsilon_{SiO2}=2.25$ and its diameter fits in with the diameter of the match end's circular cut edge (cf. Fig. 2). Figure 6 displays the electric field strength at the apex of the nanomatch (i.e., the match end's bulge) as a function of the wavelength for various matchstick lengths l and for y-polarization. Here, the cut depth h is assumed to be equal to 10 nm, rendering the match end a hemisphere where the resulting diameter of the joint matchstick amounts to 20 nm. The electric field strength at resonance increases slightly with the growing matchstick length l, reaching a maximum at the apex for l around 200 nm. This is partially due to mode interaction at the proper junction between the metal and dielectric matchstick, involving the mode supported by matchstick as well as the localized mode on the match end at which a pronounced charge accumulation is induced by this process. Interestingly for longer matchsticks (i.e., $l>600$ nm) the field enhancement saturates at a constant level, indicating that the metallic hemisphere plays the essential part with respect to the field enhancement due to the excitation of surface plasmon resonances. As observed in Fig. 6 the resonance wavelength of the match end with a cut depth of $h=10$ nm is shifted only by a few nanometers while adding the dielectric matchstick to the structure, confirming the dominant influence of the match end on the spectral response of the field enhancement. In contrast, the resonance of the nanomatch seems to be significantly influenced by the contact geometry at the proper joint. A transversal misalignment between the match end and matchstick of about 5 nm will already yield an observable shift in the resonance wavelength. This happens quite often during experiments where a metallic particle is manually attached to an atomic force microscope tip [24], especially when the extent of the nanoparticle is larger than the tip's apex. To conclude, the nanomatch structure described above turns out to be well suited as an efficient nanotip in, e.g., scanning near field microscopy measurements. One of the main advantages for such measurements lies in that the geometry of the structure can be precisely controlled during fabrications; thus the uncertainties caused by manual operations [24] could be reduced to the utmost extent. Due to the clearly defined geometry, reproducibility could be maintained if the tip was damaged during experiments, and one has to replace another tip to continue doing measurements. On the other hand, it has been recently reported that some experiments still lack in reproducibility also when similar tips were adopted [25,26].

C. Nanomatch with a Cylindrical Metallic Matchstick

In the framework of the specific fabrication technology such as nanorobotic spot welding the material of the matchstick can be easily varied during processing [8]. As observed in earlier studies metallic nanorods yield larger SCSs at optical frequencies than dielectric nanorods having the same dimensions [27]. Hence it would be interesting to investigate the variations of the optical properties of the nanomatch structure when the dielectric matchstick is replaced with a nanorod made of gold. For the first nanomatch in the subsequent analysis a match end with a diameter of 20 nm and a cut depth of $h=2$ nm has been chosen yielding a diameter of 12 nm for the cylindrical matchstick when following geometrical relation (1). The spectral response of the electric field strength at the match end's apex is shown in Fig. 7(a) for different matchstick lengths. The electric field increases significantly for matchstick lengths starting at 20 nm and continues to increase until the length reaches a value of about 100 nm. This is in conjunction with a strong redshift of the dipole resonance, which is actually not captured by the chosen frequency range in Fig. 7(a). For $l>500$ nm the field enhancement slightly decreases to an almost constant level. The appearance of several higher-order resonances is indicated in the wavelength range of interest for matchstick lengths $l>70$ nm. These additional resonances are actually based on mode coupling effects between the resonant fields on the match end and the matchstick.

The aforementioned mode coupling involves, e.g., dipole-dipole interactions at a wavelength of 520 nm [cf. Fig. 8(a)] and dipole-multipole interactions at 522 nm [cf. Fig. 8(b)], whereas an overall dipole behavior of the nanomatch to the impinging field is observed for a wavelength of 800 nm [cf. Figs. 8(a) and 8(b)]. Note that for cut

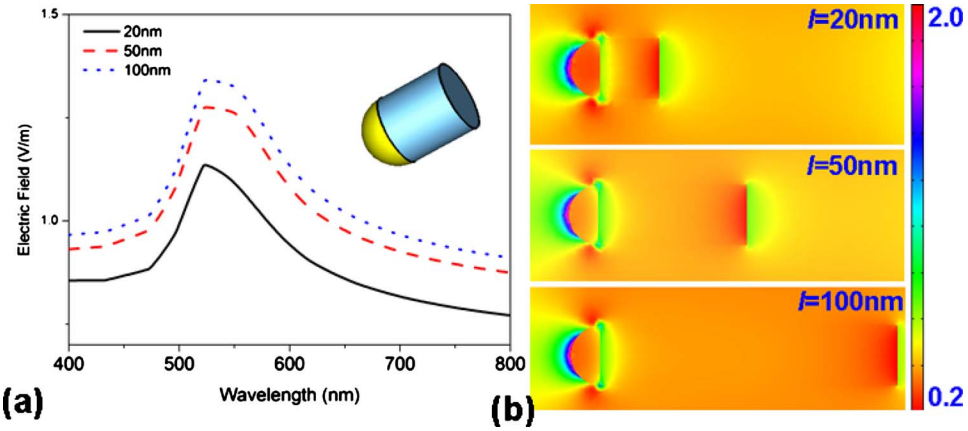

Fig. 6. (Color online) (a) The spectral response of the electric field strength as a function of the silica matchstick's lengths $l=20$, 50, 100 nm for a wavelength range between 400 and 800 nm. Inset shows the calculated structure; the metallic match end has a cut depth of $h=10$ nm ($R=10$ nm, $r=10$ nm). (b) Distribution of the electric field strength at the corresponding resonance of the resulting nanomatch under y-polarization.

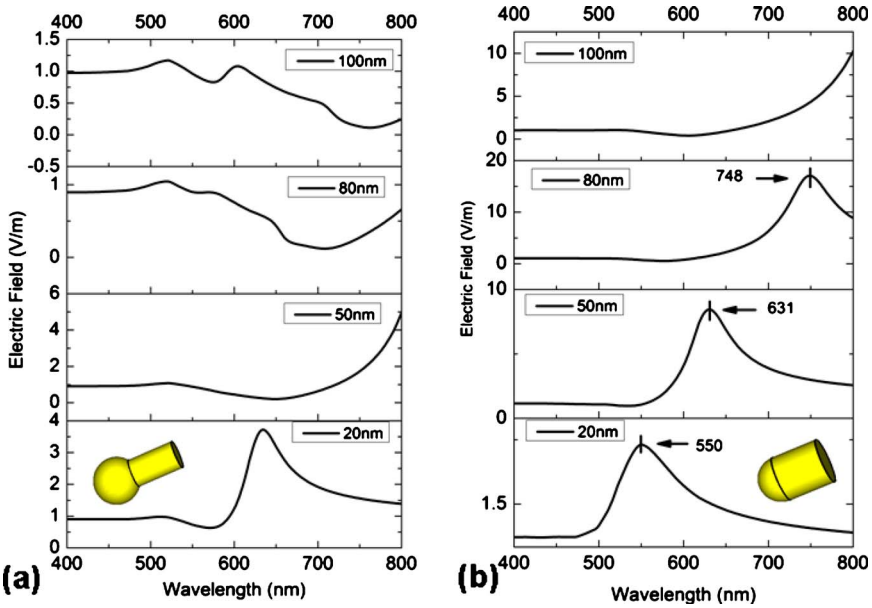

Fig. 7. (Color online) The spectral response of the electric field strength at the apex of the match end as a function of the metallic matchstick's lengths $l=20$, 50, 80, 100 nm. Both the metallic match end and the matchstick consist of gold, where the latter has cut depths of (a) $h=2$ nm ($R=10$ nm, $r=6$ nm) and (b) $h=10$ nm ($R=10$ nm, $r=10$ nm). The illumination is with y-polarization.

depths $h<10$ nm, the feature size of the match end is larger than the diameter of matchstick; hence, the field strength at the apex of match end is merely governed by the charge distribution on the truncated nanosphere, yielding only minor variations in the field enhancement at resonance. The situation is different for cut depths $h \geq 10$ nm, where the diameter of the matchstick is equal or even larger than the lateral extent of the metallic match end. In this regard Fig. 7(b) displays the spectral response of the electric field strength at the apex of the match end for a cut depth of $h=10$ nm as well as for growing stick lengths l yielding field strengths at redshifted resonances that are significantly increased. The redshift due to increasing matchstick length is in perfect agreement with classical antenna theory that has been already translated into the realm of optical dipole antennas [28].

D. Nanomatch with a Conical Metallic Matchstick

Both nanomatch configurations, namely, the one with a dielectric and with a metallic matchstick support highly tunable plasmon resonances. Nevertheless, when the extent of the match end gets larger than the diameter of matchstick, the field enhancement due to localized surface plasmons is still poor even for structures with a metallic matchstick. A large field enhancement is, however, indispensable in some applications such as sensing [2,17] and the TERS experiments [17] in order to improve the detection resolution. Therefore, some additional mechanisms, which may not be directly related to the surface plasmon resonances, such as, e.g., the "lighting rod effect" [29] could be introduced into the nanomatch topology. A simple way to realize the aforementioned idea is to use a conical metallic matchstick as shown in the inset of Fig. 9.

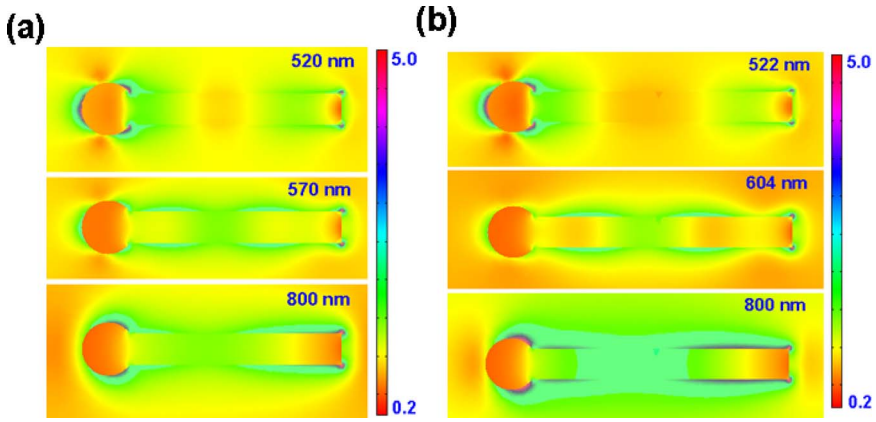

Fig. 8. (Color online) Distribution of the electric field strength for the resonant metallic nanomatches with different matchstick lengths (a) $l=80$ nm and (b) $l=100$ nm. The match end has a cut depth of $h=2$ nm and the overall nanomatch consists of gold. The illumination is with y-polarization.

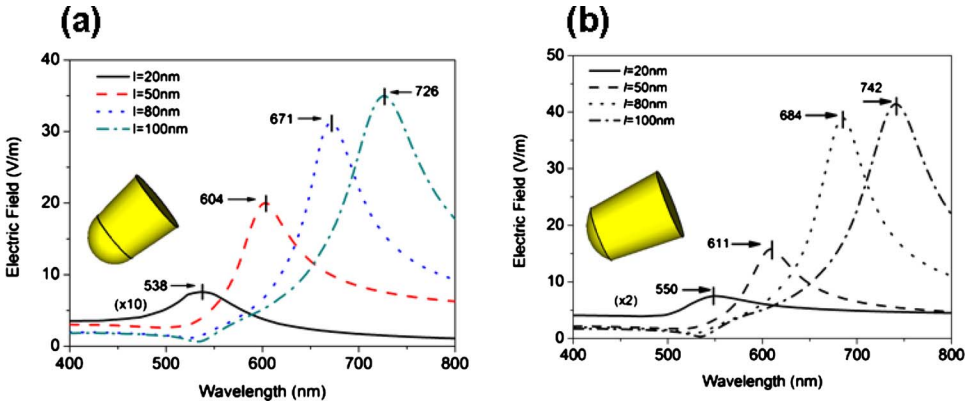

Fig. 9. (Color online) The spectral response of the electric field strength at the apex of the match end as a function of the metallic matchstick's lengths $l=20$, 50, 80, 100 nm. Both the metallic match end and the conical matchstick (full-angle 12°) consist of gold, where the latter has cut depths of (a) $h=10$ nm ($R=10$ nm, $r=10$ nm) and (b) $h=16$ nm ($R=10$ nm, $r=8$ nm). The truncated cone in (b) yields a smaller facet at the proper joint with a lateral extent of 16 nm instead of 20 nm as in (a). The illumination is with y-polarization.

In order to maintain the matchstick's outline characteristics the conical shape should comply with an acute angle. The full angle of the truncated cone is set to 12° where the smaller facet has a lateral extent of 20 nm allowing a precise joint to the hemispherical match end with a cut depth of 10 nm. This conical structure is similar to the nanotips, which are widely used in scanning near field microscopy and TERS [17,30]. In our numerical simulations we use gold as the underlying material for both the match end and matchstick. The electric field strength at the tip apex as a function of wavelength is shown in Fig. 9(a). Interestingly, five to ten times larger field enhancements were observed at the match end for conical shapes with even small acute angles compared to nanomatches with cylindrical matchsticks as depicted in Fig. 7(b). In principle further field enhancement is feasible with a reduced tip size in conjunction with an optimal conical angle, where atomic resolution is in principle accessible for tip diameters in the range of 1–2 nm [31]. However, conical nanomatch topologies with such tiny match ends are not producible with our fabrication technology [8]. The limit of the tip diameters in the case of conical nanomatch topologies that is accessible with the developed nanomatch fabrication technique is about 15 nm. An interesting workaround consists of increasing the cut depth h to, e.g., 16 nm resulting in a slight reduction in the smaller facet's lateral extent. The tip-like region of the nanomatch encompasses a circular wedge, from which we expect a ring-shaped charge accumulation due to the lightning rod effect. Interestingly, this charge accumulation in conjunction with the conical outline of the overall nanomatch seems to repulse some further charges into the tip's apex. The spectral response of the resulting maximal electric field strength is depicted in Fig. 9(b) where a five times larger field enhancement is observed for $l=20$ nm and a 1.2 times larger field enhancement for $l=100$ nm compared to the corresponding values for the cylindrical nanomatch [Fig. 9(a)]. Further improvements are expected from loss reduction when using silver instead of gold. Future research has to focus on the combination of the two metals, because such composite nanostructures may offer additional degrees of freedom for tackling tuning issues of the underlying plasmon resonances together with other concerns like, e.g., a large field enhancement. In this way the resonance tuning range from visible to near infrared can be reached.

It is worth mentioning that within all the previous simulations we have excluded the case of an infinitely long matchstick for obvious reasons. In practice, a very long matchstick is needed when looking to realistic experimental settings involving nanotips. A test model to approximate the infinite extent of a conical nanomatch has been carried out where the fat end of the metallic matchstick was directly mounted on a PML. The emergent resonances become much weaker where a flat baseline dominates the long wavelength range. The main (lowest order) resonance reached a relatively constant value when the length of the match stick is more than 10 μm in our simulation. This is coinciding with the experimental observations when an infinitely long metallic nanotip is used. It also should be pointed out here that directly mounting the metallic matchstick onto a PML would cause some numerical problems (i.e., interference patterns at the truncated matchstick end, high fields, etc.) due to the impedance mismatches between adjacent boundaries: the reflections between metal and PML are present and this might influence the calculation results a lot. One then has to choose the matchstick as much as possible to avoid the spurious reflections so that accurate results coinciding with experiments can be obtained.

A final issue concerns the involved material models. In our simulations realistic models for pure metals and dielectrics have been used, which may considerably deviate from experimental results due to stoichiometric mixing effects at the apparent material interfaces. The formation of alloys in the interface regions highly depends on the processing parameters of the underlying fabrication technology, rendering any modeling effort to become strongly reliant on preliminary material characterization such as, e.g., energy filtered TEM. With respect to, e.g., a gold/semiconductor (InAs) interface we recently observed significant indium migration from the matchstick into the gold hemisphere, leading to an estimated relative detuning of the localized surface plasmon on the order of 10% [31]. This very approximate value illustrates a fundamental complication, namely, that any modeling effort is in-

herently compromised by the lack of reliable optical material models for such specific alloys, whereas the alloy formation is a very local product of the underlying processing history.

5. CONCLUSIONS

We numerically investigated the optical properties of a newly fabricated composite wire structure—the nanomatch. A finite-difference time-domain (FDTD) method has been used and the numerical analysis has demonstrated that such a plasmonic nanostructure could be functionalized to support reliable optical properties, such as, e.g., negligible detuning when the cut depth of the match end is considerably small. Larger resonance shifts can be found when the matchstick of a corresponding length is introduced. Our research revealed that the nanomatch is eligible for various applications in the field of, e.g., sensing and provides a novel scheme for highly reproducible tips in scanning near field optical microscopy and tip-enhanced Raman spectroscopy (TERS). Further research will explore the applicability of the nanomatch in the context of short-range energy channeling as well as its implementation as nanoelectrodes in future nanophotonic circuits.

REFERENCES

1. U. Kreibig and M. Vollmer, *Optical Properties of Metal Clusters* (Springer-Verlag, 1995).
2. F. Tam, C. Moran, and N. Halas, "Geometrical parameters controlling sensitivity of nanoshell plasmon resonances to changes in dielectric environment," J. Phys. Chem. B **108**, 17290–17294 (2004).
3. C. Loo, A. Lin, L. Hirsch, M. Lee, J. Barton, N. Halas, J. West, and R. Dreyek, "Nanoshell-enabled photonics-based imaging and therapy of cancer," Technol. Cancer Res. Treat. **3**, 33–40 (2004).
4. N. Halas, "Playing with plasmons: Tuning the optical resonant properties of metallic nanoshells," MRS Bull. **30**, 362–367 (2005).
5. Z. Wu, J. Xiang, C. Yang, W. Lu, and C. M. Lieber, "Single-crystal metallic nanowires and metal/semiconductor nanowire heterostructures," Nature **430**, 61–65 (2004).
6. L. J. Lauhon, M. S. Gudiksen, C. L. Wang, and C. M. Lieber, "Epitaxial core-shell and core-multishell nanowire heterostructures," Nature **420**, 57–61 (2002).
7. F. S. Ou, M. M. Shaijumon, L. J. Ci, D. Benicewicz, R. Vajtai, and P. M. Ajayan, "Multisegmented one dimensional hybrid structures of carbon nanotubes and metal nanowires," Appl. Phys. Lett. **89**, 243122 (2006).
8. L. X. Dong, X. Y. Tao, L. Zhang, B. J. Nelson, and X. B. Zhang, "Nanorobotic spot welding: Controlled metal deposition with attogram precision from copper-filled carbon nanotubes," Nano Lett. **7**, 58–63 (2007).
9. H. Wang, D. W. Brandl, F. Le, P. Nordlander, and N. J. Halas, "Nanorice: A hybrid plasmonic nanostructure," Nano Lett. **6**, 827–832 (2006).
10. C. Charnay, A. Lee, S. Man, C. E. Moran, C. Radloff, R. K. Bradley, and N. J. Halas, "Reduced symmetry metallodielectric nanoparticles: Synthesis and plasmonic properties," J. Phys. Chem. B **107**, 7327–7333 (2003).
11. J. Ye, P. V. Dorpe, W. V. Roy, K. Lodewijks, I. D. Vlaminck, G. Maes, and G. Borghs, "Fabrication and optical properties of gold semishells," J. Phys. Chem. C **113**, 3110–3115 (2009).
12. Y. Lu, G. L. Liu, J. Kim, Y. X. Mejia, and L. P. Lee, "Nanophotonic crescent moonstructures with sharp edge for ultrasensitive biomolecular detection by local electromagnetic field enhancement effect," Nano Lett. **5**, 119–124 (2005).
13. S. Kim, K. L. Shuford, H. M. Bok, S. K. Kim, and S. H. Park, "Intraparticle surface plasmon coupling in quasi one dimensional nanostructures," Nano Lett. **8**, 800–804 (2008).
14. X. Wang and C. S. Ozkan, "Multisegment nanowire sensors for the detection of DNA molecules," Nano Lett. **8**, 398–404 (2008).
15. L. Qin, S. Park, L. Huang, and C. A. Mirkin, "On-wire lithography," Science **309**, 113–115 (2005).
16. www.cst.com.
17. W. H. Zhang, T. Schmid, B. S. Yeo, and R. Zenobi, "Single molecule tip-enhanced Raman spectroscopy with silver tips," J. Phys. Chem. C **111**, 1733–1738 (2007).
18. A. Taflove and S. C. Hagness, *Computational Electrodynamics: The Finite Difference Time Domain Method* (Artech House, 2005).
19. Y. Hao and C. J. Railton, "Analyzing electromagnetic structures with curved boundaries on Cartesian FDTD meshes," IEEE Trans. Microwave Theory Tech. **46**, 82–88 (1998).
20. N. Kaneda, B. Houshmand, and T. Itoh, "FDTD analysis of dielectric resonators with curved surfaces," IEEE Trans. Microwave Theory Tech. **45**, 1645–1649 (1997).
21. P. B. Johnson and R. W. Christy, "Optical constants of the noble metals," Phys. Rev. B **6**, 4370–4379 (1972).
22. A. Sutradhar, G. H. Paulino, and L. J. Gray, *Symmetric Galerkin Boundary Element Method* (Springer-Verlag, 2008).
23. E. Prodan, C. Radloff, N. J. Halas, and P. Nordlander, "A hybridization model for the plasmon response of complex nanostructures," Science **302**, 419–422 (2003).
24. P. Anger, P. Bharadwaj, and L. Novotny, "Enhancement and quenching of single molecule fluorescence," Phys. Rev. Lett. **96**, 113002 (2006).
25. A. Dereux, E. Devaux, J. C. Weeber, J. P. Goudonnet, and C. Girard, "Direct interpretation of near-field optical images," J. Microsc. **202**, 320–331 (2000).
26. Z. L. Wang, *Nanowires and Nanobelts: Metal and Semiconductor Nanowires* (Birkhaeuser, 2005).
27. L. Novotny, "Effective wavelength scaling for optical antennas," Phys. Rev. Lett. **98**, 266802 (2007).
28. A. V. Zayats, "Electromagnetic field enhancement in the context of apertureless near field microscopy," Opt. Commun. **161**, 156–162 (1999).
29. X. Cui, W. Zhang, B. Yeo, R. Zenobi, Ch. Hafner, and D. Erni, "Tuning the resonance frequency of Ag-coated dielectric tips," Opt. Express **15**, 8309–8316 (2007).
30. A. Downes, D. Salter, and A. Elfick, "Simulations of atomic resolution tip-enhanced optical microscopy," Opt. Express **14**, 11324–11329 (2006).
31. X. Cui and D. Erni, "The influence of particle shapes on the optical response of nearly touching plasmonic nanoparticle dimers," J. Comput. Theor. Nanosci. **7**, 1610–1615 (2010).